 doi:10.20944/preprints202107.0466.v1

Article

Obtention and Characterization of Ferrous Chloride $FeCl_2{\cdot}4H_2O$ from Pickling Waste Liquors

Lorena Alcaraz [1,*], Belén Sotillo [2], José F. Marco [3], Francisco J. Alguacil [1], Paloma Fernández [2] and Félix A. López [1]

[1] Centro Nacional de Investigaciones Metalúrgicas (CENIM), Consejo Superior de Investigaciones Científicas (CSIC), Avda. Gregorio del Amo, 8, 28040 Madrid, España; alcaraz@cenim.csic.es; fjalgua@cenim.csic.es; f.lopez@csic.es

[2] Departamento de Física de Materiales, Facultad de Ciencias Físicas, Universidad Complutense de Madrid (UCM), 28040 Madrid, España; bsotillo@fis.ucm.es; arana@fis.ucm.es

[3] Instituto de Química Física 'Rocasolano', Consejo Superior de Investigaciones Científicas (CSIC), C/Serrano, 119, 28006 Madrid, España; jfmarco@iqfr.csic.es

* Correspondence: alcaraz@cenim.csic.es

Abstract: As a hazardous waste, pickling waste liquor must be properly treated. An alternative consists in promoting the formation of ferrous salts from this residue, due to its higher ferrous content. Since $FeCl_2{\cdot}4H_2O$ is widely used in several applications, obtaining pure crystals of this material appears to be an interesting prospect. However, this compound has scarcely been investigated. In the present work, $FeCl_2{\cdot}4H_2O$ crystals have been obtained from pickling waste liquors. Their structural and morphological characteristics have been investigated by X-ray diffraction, scanning electron microscopy as well as Mössbauer spectroscopy. In addition, the photoluminescence study of the obtained samples was also assessed. It was observed that after some aging time, the obtained crystals change in colour from green to more yellowish. So, the aged sample has also been evaluated, and their structural characteristics are compared with the original crystals. Despite this, the obtained crystals exhibit a $FeCl_2{\cdot}4H_2O$ structure, which is not modified with the aging of the sample.

Keywords: Ferrous chloride; $FeCl_2{\cdot}4H_2O$ crystals; pickling waste liquors

1. Introduction

Pickling waste liquor is a common waste generated in the process of steel pickling and electroplating industry, which usually contains an acid (cleaning reagent) and a large amount of iron ions in its composition [1,2]. Normally, cleaning agents such as hydrochloric, sulphuric, hydrofluoric, and nitric acids are widely used in the mentioned process [1]. Due to the acidic nature (30-100 g/L concentration of acid), and the high concentration of iron ions (at around 60-250 g/L), this type of waste can lead to severe environmental damage and it has been listed as hazardous waste [2]. For this reason, an adequate treatment for pickling waste liquors is of great importance [3,4].

Several techniques have been used to treat pickling waste liquor including electrodialysis [5], evaporation [6], crystallization [7], selective precipitation [8], neutralization [5], or ion exchange [9]. In addition, previous investigations have reported the obtention of functional materials from the pickling waste liquors such as magnetic biochar [10], composites inorganic coagulants [8], or ferrites [12,13].

Another recovery alternative is the direct conversion of the unused acid to its corresponding iron salt [14]. Among the different ferrous salts, there is a great interest in the $FeX_2{\cdot}4H_2O$ systems, especially $FeCl_2{\cdot}4H_2O$, due to their potential applications in chemistry and composite material areas [15]. $FeCl_2{\cdot}4H_2O$ is useful used as reducing [16,17] and electrolytic agent [18], synthesis of pharmaceutical compounds [19,20], or water treatment [21,22].

Preprints (www.preprints.org) | NOT PEER-REVIEWED | Posted: 20 July 2021 doi:10.20944/preprints202107.0466.v1

Despite ferrous chloride has been obtained from pickling waste liquors, to the best of our knowledge, the structural characterization of $FeCl_4 \cdot 4H_2O$ has been scarcely investigated. In the present work, the obtention of $FeCl_2 \cdot 4H_2O$ from pickling waste liquor using an effective process is described. A deep characterization of the structural and optical properties of the obtained samples was performed. In addition, the effects of aging on the crystal structure, structural characteristics as well as optical properties have been carried out.

2. Experimental

2.1. Obtention of the iron chloride from pickling waste liquor

Ferrous chloride was obtained from pickling waste liquor from hydrochloric acid (HCl) pickling process of carbon steel.

Acid pickling with HCl is a chemical process aimed at dissolving iron oxides from the metal surface without any significant attack on the steel. The oxidation layer composed of different types of iron oxides (Fe_2O_3, Fe_3O_4, and FeO) reacts with HCl to form ferrous chloride through reactions 1-3 [23]. Meanwhile, hydrochloric acid penetrates the oxidation layer and attacks the underlying metal. Ferrous chloride and hydrogen gas are produced by the reaction between hydrochloric acid and base steel (reaction 4) [23]. Due to these reactions, the oxidized layer is peeled off the surface, which is the main action of the pickling process.

$$Fe_2O_3 + Fe + 6HCl \rightarrow 3FeCl_2 + 3H_2O \quad (1)$$
$$Fe_3O_4 + Fe + 8HCl \rightarrow 4FeCl_2 + 4H_2O \quad (2)$$
$$FeO + 2HCl \rightarrow FeCl_2 + H_2O \quad (3)$$
$$Fe + 2HCl \rightarrow FeCl_2 + H_2 \quad (4)$$

When free HCl is exhausted and ferrous chloride accumulates in the pickling liquor to the point where pickling cannot be carried out effectively, spent pickling solutions are discharged from the pickling tanks and managed as hazardous waste. It is estimated that around 380,000 m^3 of chlorinated pickling water is produced annually in Europe [24]. One way to utilize this water is to treat it to recover the ferrous chloride and residual acid.

The pickling water used in this work comes from the company HIASA (Asturias, Spain). The pickling water (139.9±5.1 g/L Fe^{2+}, 43.6±8.2 g/L free acid, 237.5±20.5 g/L total acid) was treated in a pilot evaporation-crystallization plant. The pickling water was heated to 130 °C in a pre-heater before entering a 500 mm long Vigreux column at the same temperature. The pickling water inlet flow into the column was 3 L/h. In the column, the pickling water is split into two streams: a vapour stream that condenses in a condenser at 65 °C and a liquor enriched in Fe^{2+} (188 ± 8.6 g/L). The vapour leaving the Vigreux column is split into two streams in the condenser. A concentrated acid stream (107.7± 21.8 g/L) and a water stream which is treated in a condenser at 6 °C to obtain a water stream without free acid. The whole system is kept under a vacuum of -640 mbar. The enriched liquor is crystallized in a crystallizer at 130 °C and filtered to obtain a mass of crystallized ferrous chloride and a residual solution that was recirculated at the beginning of the process. Figure 1 shows the ferrous chloride crystals immediately after crystallization and filtration. Concentrated acid and water can be reused in the pickling process.

Preprints (www.preprints.org) | NOT PEER-REVIEWED | Posted: 20 July 2021 doi:10.20944/preprints202107.0466.v1

Figure 1. Ferrous chloride crystals obtained from pickling waste liquor by the described method.

2.2. Characterization of the iron chloride obtained from pickling waste liquor

X-ray diffraction measurements (XRD) have been done using a PANalytical Empyrean diffractometer using λ Cu Kα radiation with a step size of 0.02° (2θ) and a step time of 7.9 s. Powder diffraction data were refined by the Rietveld method using the FullProf software [25].

Micro-Raman measurements were performed at room temperature in a Horiba Jobin Yvon LabRAM HR800 confocal microscope. Raman spectra were recorded under excitation with the 632.8 nm line of a He-Ne laser. A charge-coupled device (CCD) detector was used to collect the scattered light dispersed by a 600 lines/mm grating. The spectral resolution of the system used was 1.5 cm^{-1}. Photoluminescence measurements were done in the same system but using the 325 nm line of a He-Cd laser as excitation source.

Optical micrographs were taken using a Leica DFC295 digital camera mounted on a Leica MSV266 microscope.

The morphology and chemical composition of the obtained crystals were carried out by Field Emission Scanning Electronic Microscopy using a Hitachi S-4800 and a FEI Inspect SEM.

^{57}Fe Mössbauer data were recorded at 298 K in the transmission mode using a conventional constant acceleration spectrometer and a ^{57}Co(Rh) source. An effective absorber thickness of *ca*. 5 $mg \cdot cm^{-2}$ of natural iron was used in all the cases. The velocity scale was calibrated using a 6 μm thick iron foil. The isomer shifts were referred to the centroid of the spectrum of α-Fe at room temperature. All the spectra were computer-fitted using Lorentzian lines.

3. Results and discussion

Commercial ferrous chloride (CFC) was analyzed for comparison purposes (Figure 2a). The fresh sample (CFF) was aged for a few days (CFT) at standard conditions (around 298 K, and 100 kPa of pressure). The initial light-green colour of the sample (Figure 2b) was turned to brown in some areas of the obtained crystals (Figure 2c-d). The change in colour from green to more yellowish crystals occurring in a few days (figure 2c). If the samples are left in ambient atmosphere for more than 20 days, the colour progresses towards an orange-brown (Figure 2b-d). No further changes are observed in samples aged for months, indicating that at some point the degradation of the crystals stops. A close inspection of the samples shows that orange regions and orange agglomerates appear between and on the crystals, respectively (Figure 2d). Moreover, although the crystals are still green in colour, they lost their transparency and the surface is much rougher. These two effects are behind the macroscopic colour change observed in the aged samples.

Preprints (www.preprints.org) | NOT PEER-REVIEWED | Posted: 20 July 2021 doi:10.20944/preprints202107.0466.v1

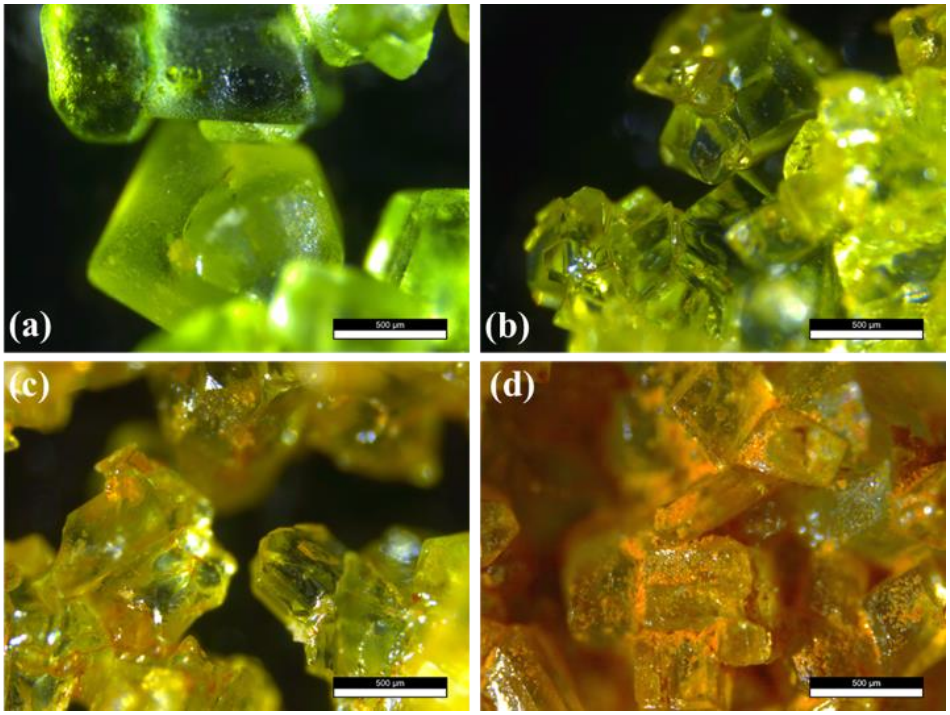

Figure 2. Optical micrographs of the $FeCl_2 \cdot 4H_2O$ crystals: (a) Commercial reference crystals (CFC). (b) Fresh $FeCl_2 \cdot 4H_2O$ sample (CFF). (c)-(d) Images showing different stages of the aging of the crystals (CFT): (c) few days; (d) months. In all cases, the scale bar is 500 μm.

3.1. X-ray diffraction (XRD)

Figure 3 exhibits comparative X-ray diffraction patterns of the samples investigated. All diffraction maxima can be indexed to a monoclinic structure with a space group $P2_1/c$ and Z = 2 (14) (PDF 01-071-0668) compatible with a $FeCl_2 \cdot 4H_2O$ phase. No additional peaks were observed within the sensitivity of the experimental system used indicating the purity of the obtained samples. Lower intensity diffraction maxima can be observed in the difractogram of the CFC sample, as compared with that of the CFF sample. This result could be indicating the presence of an amorphous phase/thin layer of degradation products formed on the surface of the aged sample which goes undetected by XRD. The possible formation of this thin layer on the surface of ferrous chloride crystals would lead to a decrease of the diffraction maxima intensity. It should be noted that optical images exhibit a colour change in some areas of the CFF sample (see figure 2c, and figure 2d).

Preprints (www.preprints.org) | NOT PEER-REVIEWED | Posted: 20 July 2021 doi:10.20944/preprints202107.0466.v1

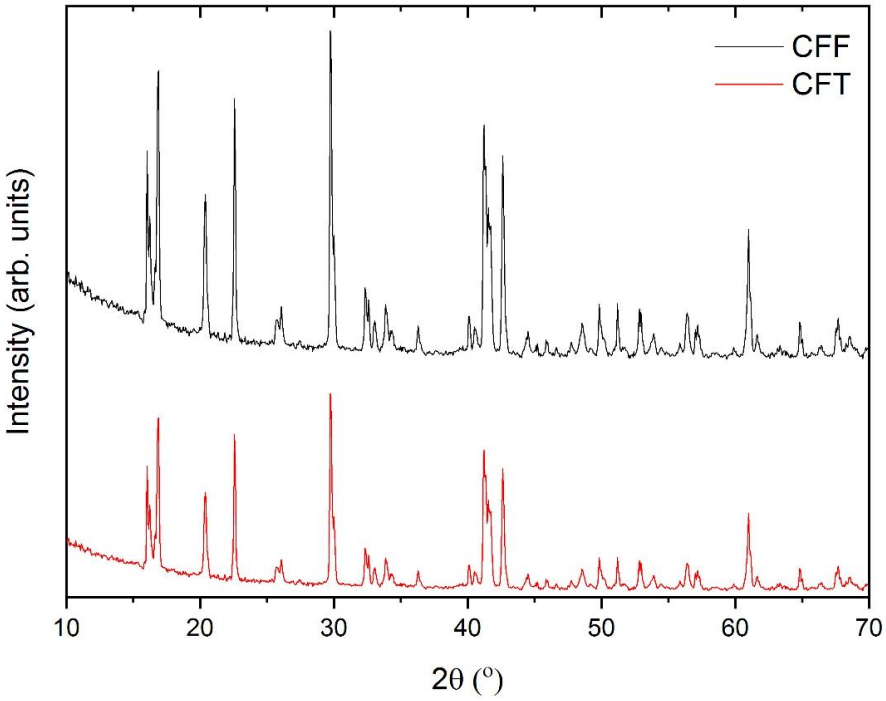

Figure 3. XRD patterns of the obtained ferrous chloride samples.

In order to carry out a more detailed structural characterization, XRD data were refined by the Rietveld method where iron atoms were distributed in the 2a (0, 0, 0) positions, and chlorine, oxygen, and hydrogen were located in the 4e (x, y, z) sites. FulProf software was used to calculate the structural parameters of the samples according to the crystallographic database code ICSD-9198 [26]. Lattice parameters and cell angles of the obtained samples are shown in Table 1. Slight differences were found in the calculated cell parameters (i.e. cell parameters, and cell angles) for both, CFF and CFT, ferrous chloride samples. In addition, these values are similar to previously reported, as well as to the theoretical values. The obtained results show that the structure of the $FeCl_2{\cdot}4H_2O$ samples obtained from the pickling waste liquors is in good accordance with the theoretical structure previously reported for this compound [26,27].

Table 1. Lattice parameters, and cell angles calculated from the Rietveld refinements for the obtained samples.

Sample	a (Å)	b (Å)	c (Å)	α (°)	β (°)	γ (°)
[26]	5.885(3)	7.174(3)	8.505(4)	90	111.11(5)	90
CFF	5.891(4)	7.117(4)	8.510(1)	90	111.10(2)	90
CFT	5.902(8)	7.121(6)	8.486(3)	90	112.02(8)	90

According to the calculated structural parameters, the crystal structure of the obtained $FeCl_2{\cdot}4H_2O$ crystals structure is formed by a net of octahedra. Each octahedron has the metal (Fe) at the center, surrounded by two Cl atoms and 4 water molecules (see Figure 4).

Preprints (www.preprints.org) | NOT PEER-REVIEWED | Posted: 20 July 2021 doi:10.20944/preprints202107.0466.v1

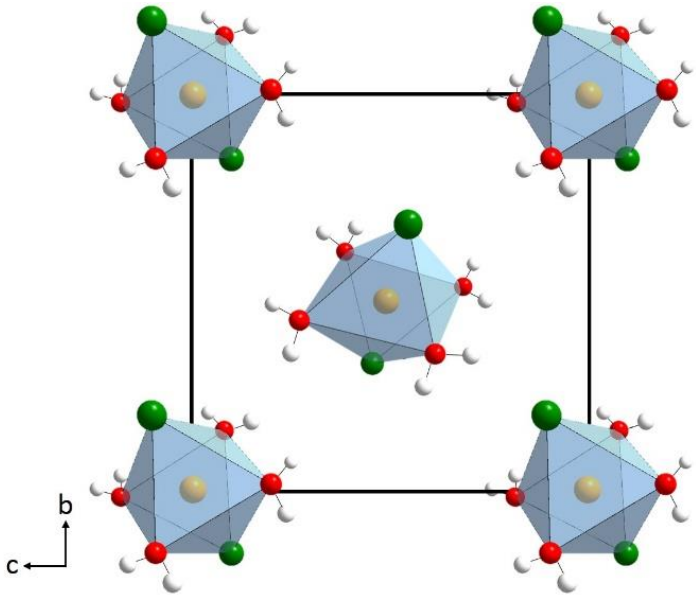

Figure 4. Crystal structure for the $FeCl_2 \cdot 4H_2O$.

3.2. Scanning electron microscopy (SEM)

Figure 5 shows the SEM images of the CFC reference sample and the obtained crystals of $FeCl_2 \cdot 4H_2O$ (CFF fresh sample, and CFT aged sample). In all cases, similar morphologies were found. SEM micrographs reveal the formation of cubic crystals, in good agreement with those previously reported for samples with the same stoichiometry [27]. However, a smoother surface was found in the case of the CFF sample (Figure 5b) as compared with the CFT sample (Figure 5c). In the latter case, some areas of the crystals exhibit a rougher surface (shown in the inset of Figure 5c), which correspond to the orange areas of the aged sample, which might be consistent with the formation of small crystallites of a new phase on the surface of the ferrous chloride crystals. These results again are in agreement with the optical images and XRD results.

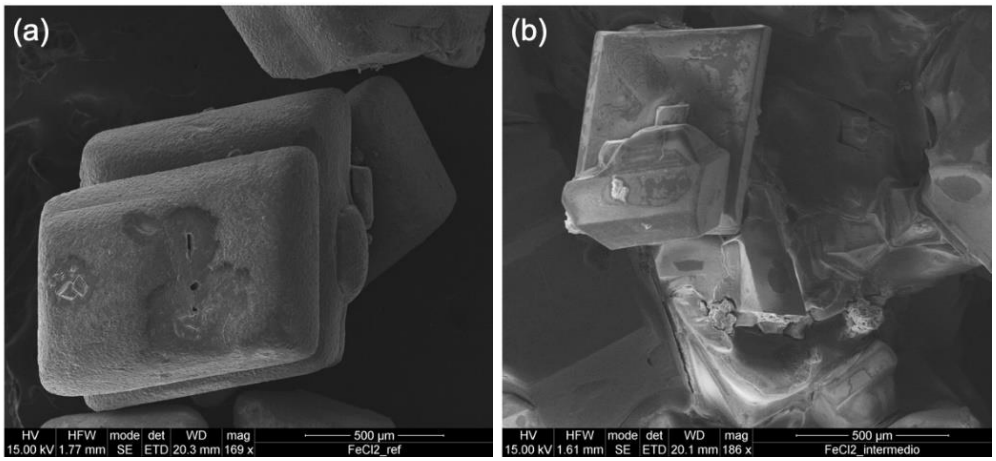

Preprints (www.preprints.org) | NOT PEER-REVIEWED | Posted: 20 July 2021 doi:10.20944/preprints202107.0466.v1

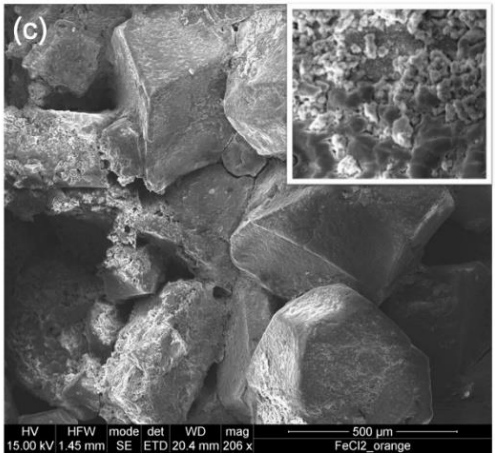

Figure 5. SEM micrographs of the (a) CFC reference sample, and (b) CFF and (c) CFT obtained crystals.

3.3. µ-Raman spectroscopy and µ-photoluminescence

In order to confirm the crystal structure of the obtained $FeCl_2{\cdot}4H_2O$ sample and study the formation of new phases in the aging process, micro-Raman spectroscopy measurements have been performed. In Figure 6, the Raman spectra of the reference FCF crystals and the fresh sample CFF are shown. In both cases (Figure 6a), all the modes can be ascribed to $FeCl_2{\cdot}4H_2O$ with monoclinic C_{2h}^5 space group [28], in agreement with the XRD results. The 30 atoms in the unit cell give rise to 42 Raman active modes. Furthermore, the observed Raman modes can be divided in different types, also related to different frequency ranges. At frequencies below 100 cm^{-1}, octahedra external modes are detected (peak at 70 cm^{-1}). The octahedra internal modes appear in the frequency range between 100 cm^{-1} and 400 cm^{-1} (Figure 6b, indicated as octahedra internal deformations, OID). The peaks at 104, 145, and 170 cm^{-1} (measured on the CFF spectrum) are related to the internal deformation bending of the octahedra. A shoulder at around 190 cm^{-1} is associated with Fe-Cl stretching modes. On the other hand, Fe-O stretching mode peaks are located at 203 and 303 cm^{-1}. The rest of the observed modes come from the vibrations of the water molecules. The band related to water vibration modes is found at 619 cm^{-1} (Figure 6a). The peaks shown in Figure 6b are ascribed to bending vibrations of the water molecules (1632 and 1651 cm^{-1}). Finally, stretching vibrations (symmetric and antisymmetric) of the water molecules are included in the band centered at 3410 cm^{-1} (Figure 6d).

Preprints (www.preprints.org) | NOT PEER-REVIEWED | Posted: 20 July 2021 doi:10.20944/preprints202107.0466.v1

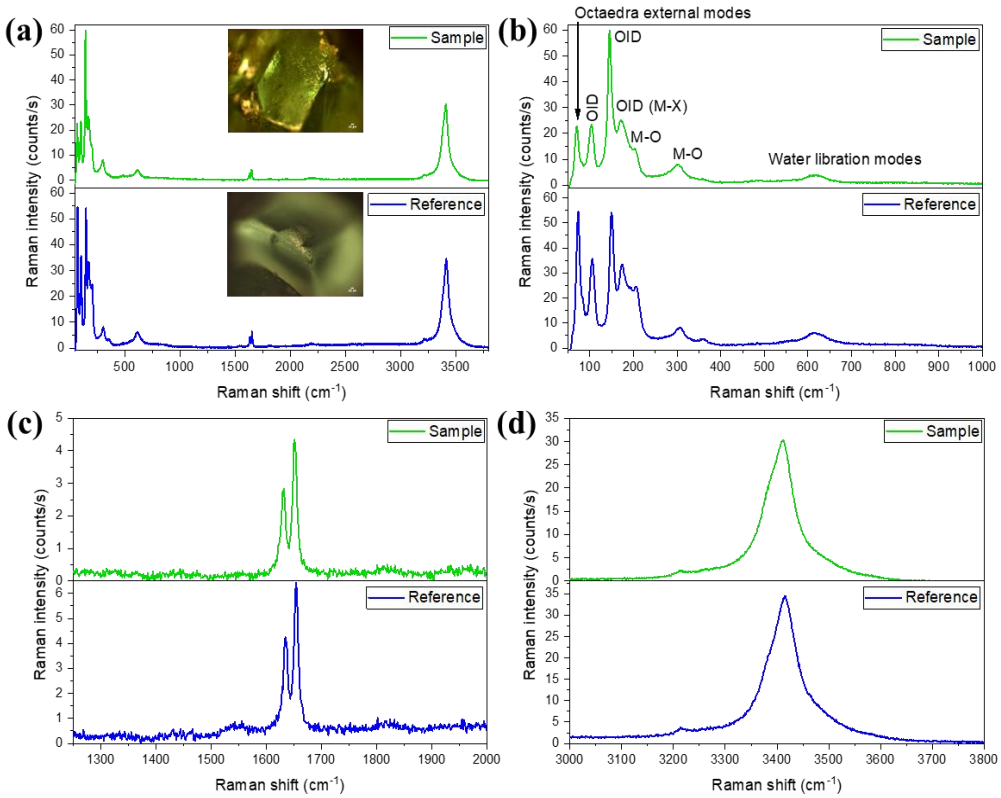

Figure 6. Micro-Raman spectra recorded on the CFC sample (blue) and the CFF sample (green). The excitation wavelength is 633 nm. (a) Spectra showing all the Raman peaks obtained. In the inset, optical images of both reference and obtained crystals are shown. (b) Raman modes appearing in the low-frequency range (50-1000 cm^{-1}). (c) Intermediate frequency range (1250-2000 cm^{-1}). (d) High-frequency range (3000-3800 cm^{-1}).

As has been already mentioned, as the colour of the samples changes from green to orange-brown, the aspect of the crystals in the optical microscope images changes (see figures 2c-d). Two different regions are observed in the CFT crystals: the region that still has a green colour and the orange region (Figure 7a). We have used micro-Raman measurements to study the differences between the green and the orange regions. The spectra recorded on the green part of the crystal (Figure 7b-c) reveal that it is still $FeCl_2{\cdot}4H_2O$, as it exhibits the same modes as those described in figure 6. The main difference is the signal intensity, which is lower in the aged samples. This can be related to a decrease in the crystal quality. On the other hand, the spectra recorded on the orange region (Figure 7d-e) are completely different. The first observation that can be made is the disappearance of the water molecule vibrations between 1600 and 3800 cm^{-1} (Figure 7c). Then, the modes are mainly found in the range between 50 and 1000 cm^{-1} (Figure 7d).

Preprints (www.preprints.org) | NOT PEER-REVIEWED | Posted: 20 July 2021 doi:10.20944/preprints202107.0466.v1

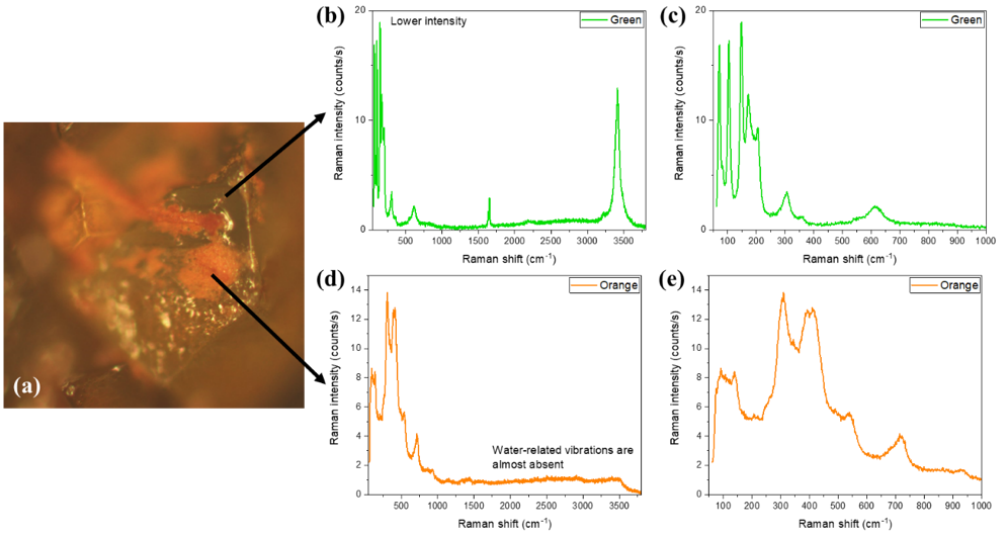

Figure 7. Micro-Raman spectra recorded on CFT sample. (a) Optical micrograph of a crystal, showing the regions where the spectra were taken. (b)-(c) Raman spectra measured on the green region. (d)-(e) Raman spectra recorded on the orange region.

Although in some rare cases a peak at 191 cm^{-1}, related to the $FeCl_3$ compound [29] can be detected (Figure 8a), the most common peaks recorded in the orange region are those shown in Figure 7e. They are broad bands centered at about 112, 305, 399, 493, 540, and 717 cm^{-1}. They can be related to different phases of iron oxyhydroxides (FeOOH) [30], specifically akaganeite (β-FeOOH) [31].

The formation of iron oxyhydroxides has been observed in the corrosion process of iron in the presence of chloride ions [32]. It has been reported [33] that when iron metals are exposed to concentrated hydrochloric acid and subsequently to a humid environment, $FeCl_2.4H_2O$ crystals are first formed. After some time, a membrane of β-FeOOH covers the ferrous chloride. β-FeOOH is commonly found on iron exposed to highly chlorinated water, or on iron immersed in strong solutions of hydrochloric acid or sodium chloride and then exposed to air [33]. A similar situation could be occurring for our crystals: first, the formation of the $FeCl_2{\cdot}4H_2O$ crystals by the as-described process, an iron compound exposed to concentrated HCl solution, and then exposed to air for few days (with the corresponding air humidity). In addition, iron chloride hydrates are deliquescent. Thus, ferrous chloride could absorb air humidity and dissolve in it, leading to a superficial film solution formed by Fe^{2+}, Cl^-, and oxygen, and promoting the oxidation of Fe(II) to Fe(III) forming the β-FeOOH phase.

For CFT samples aged for a period of months, a shaper peak at 331 cm^{-1} can also be detected in some areas (Figure 8b), which can be also related to the akaganeite phase with Cl [34]. All these results point toward the formation of akaganeite iron oxyhydroxide due to the presence of HCl on the surface of the crystals that remains after the washing process.

Preprints (www.preprints.org) | NOT PEER-REVIEWED | Posted: 20 July 2021 doi:10.20944/preprints202107.0466.v1

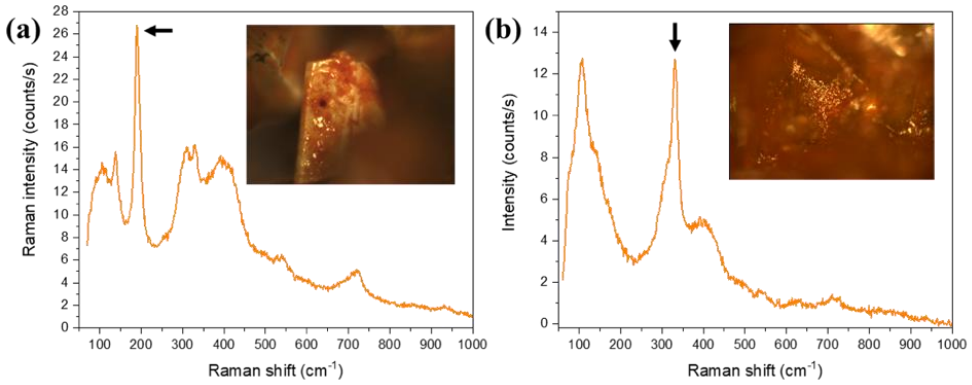

Figure 8. Micro-Raman spectra recorded on CFT sample: (a) showing the peak related to $FeCl_3$; (b) showing the peak adscribed to akaganeite phase with Cl. Insets: optical micrographs of the crystals where the spectra were taken.

Photoluminescence (PL) measurements have been also performed on both green and orange regions. Again, a clear difference in the signal recorded has been observed (Figure 9). PL spectrum of green crystals is dominated by a sharp peak at 365 nm. No reference in the literature has been found about the PL emission of $FeCl_2{\cdot}4H_2O$ compound, but the same emission is found in the CFC and CFF samples (Figure 9, blue and green line respectively). Due to the sharpness and shape of this peak, it can be related to the near band edge emission of the material. This emission disappears completely in the orange regions of the CFT sample, in agreement with the material transformation described in the Raman measurements (Figure 9, orange line).

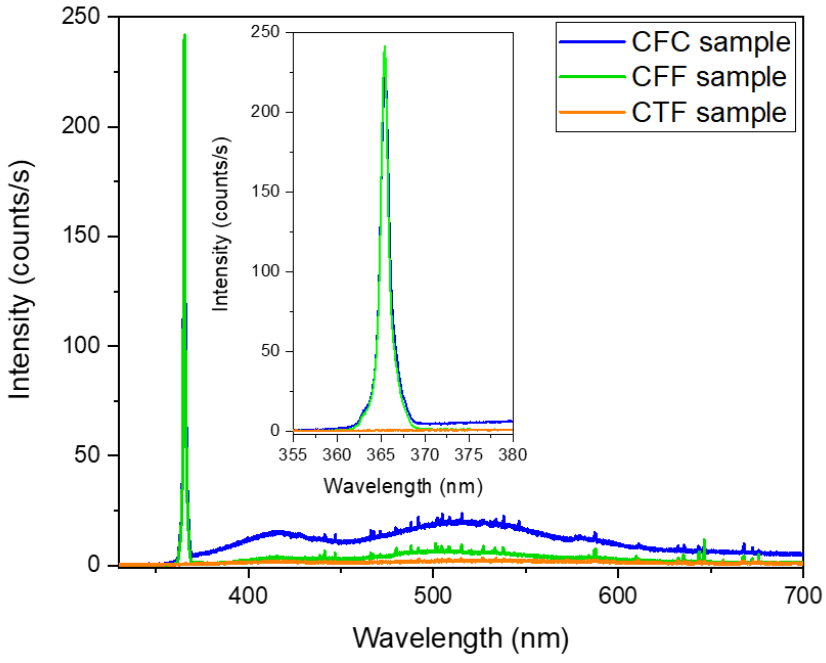

Figure 9. PL emission of CFC sample, CFF sample, and CTF sample, recorded using 325 nm laser excitation wavelength. In the inset, a zoom of the peak at 365 nm is shown.

3.4. Mössbauer spectroscopy

Figure 10 collects the 298 K ^{57}Fe Mössbauer spectra recorded from a commercial $FeCl_2{\cdot}4H_2O$ sample (CFC), a fresh sample (CFF), and a sample aged for seven days (CFT). The CFC spectrum consists of a narrow doublet with isomer shift δ=1.21 mm·s^{-1} and quadrupole splitting δ=2.98 mm·s^{-1}. These hyperfine parameters are fully characteristic of

Preprints (www.preprints.org) | NOT PEER-REVIEWED | Posted: 20 July 2021 doi:10.20944/preprints202107.0466.v1

$FeCl_2{\cdot}4H_2O$ [35]. The spectrum taken from CFF is also a narrow doublet with identical parameters to those of CFC. Therefore, we can confidently ensure that the fresh sample CFF is $FeCl_2{\cdot}4H_2O$. Differently to the spectra of these two samples, the spectrum recorded from the aged sample CFT shows two quadrupole doublets. A major one, accounting for 95% of the spectral area and parameters typical of $FeCl_2{\cdot}4H_2O$, and a minor one, 5%, with isomer shift δ=0.38 mms-1 and quadrupole splitting Δ=0.54 mms^{-1}. These Mössbauer parameters can be assigned to Fe^{3+} oxyhydroxides such as lepidocrocite (δ-FeOOH) or akaganeite (δ-FeOOH) [36]. Since akageneite is usually formed in the presence of chloride ions it is plausible to think that the Fe^{3+} doublet can be due to this latter oxyhydroxide. Also, akaganeite is the compound detected in Raman spectroscopy, as we have described before. The spectra of samples aged for longer (up to 60 days) did not show higher Fe^{3+} concentrations than that shown by CFT.

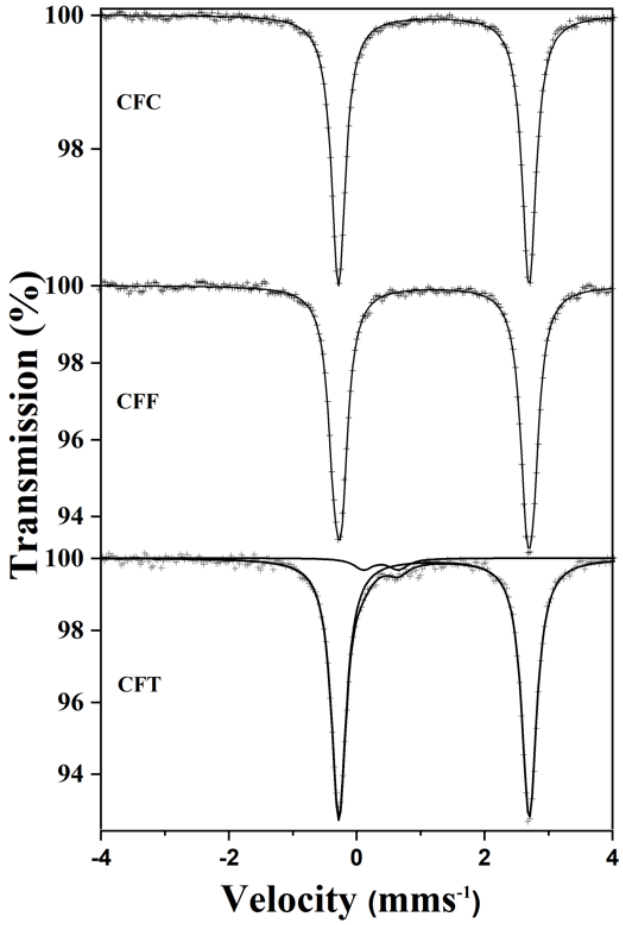

Figure 10. 298 K ^{57}Fe transmission Mössbauer spectra recorded from the various samples.

Then, the observed colour change can be related to a degradation process of the crystals due to the formation of rust on the surface and intergranular sites (Figure 2d). The rush formed is composed mainly by akaganeite iron oxyhydroxide (β-FeOOH), as confirmed by Raman and Mössbauer measurements. In the case of the sample aged for longer, the formation of a surface film of the akaganeite phase (which is not liquescent) could reduce the degradation of the ferrous crystals. For this reason, the corrosion stops when this film is enough to prevent the contact of the $FeCl_2{\cdot}4H_2O$ surface with the air humidity.

In addition, it has been possible to obtain bigger $FeCl_2{\cdot}4H_2O$ from the pickling waste liquors by the ferrous phase slowly concentrated (Figure 11a). The Raman spectrum of these crystals is the same as those described in Figure 5, confirming that they have the

Preprints (www.preprints.org) | NOT PEER-REVIEWED | Posted: 20 July 2021 doi:10.20944/preprints202107.0466.v1

same crystal structure (Figure 11b). More interesting is that these bigger crystals do not present degradation even if they are left in ambient for a long period of time. Orange agglomerates that may be found on these bigger crystals show the Raman spectrum of $FeCl_3$ compound, without modes related to the oxyhydroxides.

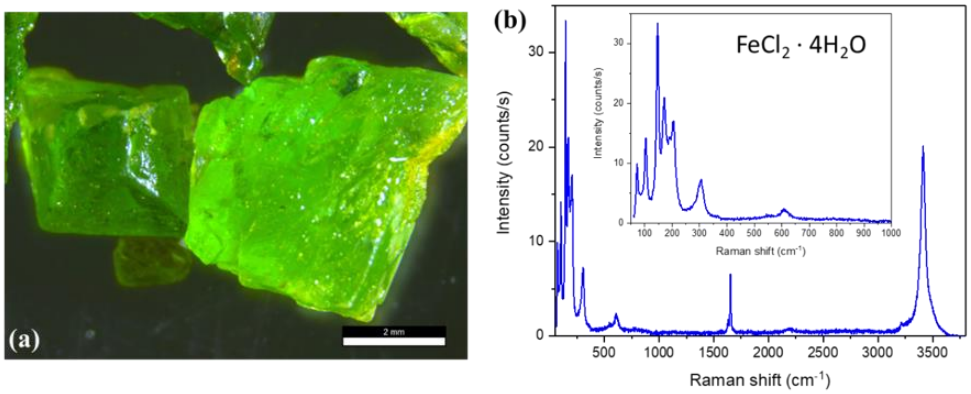

Figure 11. (a) Optical micrographs of the $FeCl_2{\cdot}4H_2O$ crystals of larger size (scale bar of 2 mm). (b) Micro-Raman spectra recorded on the crystals of part (a).

4. Conclusions

Ferrous chloride crystals with $FeCl_2{\cdot}4H_2O$ stoichiometry were obtained from liquors hydrochloric acid pickling process of carbon steel. The samples were obtained in a pilot evaporation-crystallization plant using pickling water from the company HIASA (Asturias, Spain). The final obtained crystals were characterized by a wide number of techniques. The effect of the aging of the samples in the structural characterization was also assessed. XRD shows that in both, fresh and aging samples all diffraction maxima can be attributed to the $FeCl_2{\cdot}4H_2O$ structure. In addition, the results obtained from the Rietveld refinement exhibit that the structural parameters were similar to the theoretical previously reported for this type of structure. SEM images reveal the formation of cubic crystals in all cases. Moreover, the obtained ferrous crystals exhibit a smooth surface, as in the case of the reference sample, while in the case of the aged sample some rougher surface areas were found which might be due to the formation of small crystallites of a new phase. μ-Raman spectra for the reference sample and the obtained ferrous chloride crystals were similar. All vibration modes can be attributed to $FeCl_2{\cdot}4H_2O$ phase, with monoclinic C_{2h}^5 space group. Stretching vibrations (symmetric and antisymmetric) of the water molecules in the structure were also detected. Two different Raman spectra were found in the case of the aged sample related to the different areas observed. Green regions exhibit the same Raman spectra attributable to $FeCl_2{\cdot}4H_2O$ phase. In the case of orange regions, Raman peaks that can be related to different phases of iron were found probably due to a corrosion process of iron in the presence of chloride ions in the aged sample. Differences in the intensity PL were observed for the analyzed samples. Despite that, to the best of our knowledge PL study of this type of compound has not previously been reported, the dominated sharp band could be related to the near band edge emission of the material. Mössbauer spectra of both the reference sample and the obtained crystals consists of a narrow doublet, which are fully characteristic of $FeCl_2{\cdot}4H_2O$. Again, the obtained results reveal the formation of $FeCl_2{\cdot}4H_2O$ crystals. In the case of the aged sample, the spectrum shows two quadrupole doublets. One of them accounting for 95% of the spectral area, which is typical of $FeCl_2{\cdot}4H_2O$; while the other one accounting for 5%, and can be assigned to Fe^{3+} oxyhydroxides. The spectra of samples aged for longer periods did not show higher Fe^{3+} concentrations. Thus, all obtained results reveal that it is possible to obtain high-purity and high-stability $FeCl_2{\cdot}4H_2O$ crystals from pickling waste liquors.

Author Contributions: Conceptualization, Félix López; Formal analysis, Lorena Alcaraz, Belén Sotillo, José F. Marco, Paloma Fernández and Félix López; Investigation, Lorena Alcaraz, Belén Sotillo,

José F. Marco, Paloma Fernández and Félix López; Methodology, Lorena Alcaraz, Belén Sotillo, Francisco Alguacil and Félix López; Writing – original draft, Lorena Alcaraz, Belén Sotillo and José F. Marco; Writing – review & editing, Lorena Alcaraz, Belén Sotillo, José F. Marco, Francisco Alguacil, Paloma Fernández and Félix López.

Funding: Authors from the National Center for Metallurgical Researches, Spanish National Research Council (CENIM-CSIC) would like to thank the financial support thought the project DECAPVALUE. HIASA Contract ID 20200543.

Acknowledgments: B.S. acknowledges the postdoctoral fellowship from the "Atracción de Talento" Program funded by the Comunidad de Madrid (2017-T2/IND-5465). P.F. acknowledges Complutense University of Madrid and Banco Santander for support via the project UCM-Santander 2019 (PR87/19-22613). Financial support from the Spanish Agencia Estatal de Investigación through project RTI2018-095303-B-C51 is gratefully acknowledged.

Conflicts of Interest: The authors declare no conflict of interest.

References

1. Tang, J.; Pei, Y.; Hu, Q.; Pei, D.; Xu, J. The Recycling of Ferric Salt in Steel Pickling Liquors: Preparation of Nano-sized Iron Oxide. *Procedia Environ. Sci.* **2016**, *31*, 778–784, doi:10.1016/j.proenv.2016.02.071.

2. Gao, J.; Du, Z.; Ma, S.; Cheng, F.; Li, P. High-efficiency leaching of valuable metals from saprolite laterite ore using pickling waste liquor for synthesis of spinel-type ferrites MFe_2O_4 with excellent magnetic properties. *J. Mater. Res. Technol.* **2021**, *10*, 988–1001, doi:10.1016/j.jmrt.2020.12.063.

3. Negro, C.; Blanco, P.; Dufour, J.; Latorre, R.; Formoso, A.; López, F. The treatment of hydrochloric acid waste pickle liquors. *J. Environ. Sci. Heal. . Part A Environ. Sci. Eng. Toxicol.* **1993**, *28*, 1651–1667, doi:10.1080/10934529309375969.

4. Schmidt, B.; Wolters, R.; Kaplin, J.; Schneiker, T.; Lobo-Recio, M. de los A.; López, F.; López-Delgado, A.; Alguacil, F.J. Rinse water regeneration in stainless steel pickling. *Desalination* **2007**, *211*, 64–71, doi:10.1016/j.desal.2006.03.591.

5. Hoak, R.D.; Lewis, C.J.; Hodge, W.W. Treatment of Spent Pickling Liquors with Limestone and Lime. *Ind. Eng. Chem.* **1945**, *37*, 553–559, doi:10.1021/ie50426a017.

6. Rituper, R. High-performance effluent-free pickling plants with fluid bed hydrochloric acid regeneration. *Iron Steel Eng.* **1995**, *72*, 50–54.

7. Marañón, E.; Suárez, F.; Alonso, F.; Fernández, Y.; Sastre, H. Preliminary Study of Iron Removal from Hydrochloric Pickling Liquor by Ion Exchange. *Ind. Eng. Chem. Res.* **1999**, *38*, 2782–2786, doi:10.1021/ie9806895.

8. López-Delgado, A.; Alguacil, F.J.; López, F.A. Recovery of iron from bio-oxidized sulphuric pickling waste water by precipitation as basic sulphates. *Hydrometallurgy* **1997**, *45*, 97–112, doi:10.1016/S0304-386X(96)00066-7.

9. Tomaszewska, M. Recovery of hydrochloric acid from metal pickling solutions by membrane distillation. *Sep. Purif. Technol.* **2001**, *22–23*, 591–600, doi:10.1016/S1383-5866(00)00164-7.

10. Yi, Y.; Tu, G.; Zhao, D.; Tsang, P.E.; Fang, Z. Pyrolysis of different biomass pre-impregnated with steel pickling waste liquor to prepare magnetic biochars and their use for the degradation of metronidazole. *Bioresour. Technol.* **2019**, *289*, 121613, doi:10.1016/j.biortech.2019.121613.

11. Yang, S.; Li, W.; Zhang, H.; Wen, Y.; Ni, Y. Treatment of paper mill wastewater using a composite inorganic coagulant prepared from steel mill waste pickling liquor. *Sep. Purif. Technol.* **2019**, *209*, 238–245, doi:10.1016/j.seppur.2018.07.049.

12. Ciminelli, V.S.T.; Dias, A.; Braga, H.C. Simultaneous production of impurity-free water and magnetite from steel pickling liquors by microwave-hydrothermal processing. *Hydrometallurgy* **2006**, *84*, 37–42, doi:10.1016/j.hydromet.2006.03.058.

13. Chen, D.; Hou, J.; Yao, L.; Jin, H.; Qian, G.-R.; Xu, Z.P. Ferrite materials prepared from two industrial wastes: Electroplating sludge and spent pickle liquor. *Sep. Purif. Technol.* **2010**, *75*, 210–217, doi:10.1016/j.seppur.2010.07.009.

14. Özdemir, T.; Öztin, C.; Kıncal, N.S. Treatment of waste pickling liquors: process synthesis and economicanalysis.

Chem. Eng. Commun. **2006**, *193*, 548–563, doi:10.1080/00986440500192238.

15. Zając, M.; Lipiński, I.E.; Rudowicz, C. Magnetostructural correlations for Fe^{2+} ions at orthorhombic sites in $FeCl_2 \cdot 4H_2O$ and $FeF_2 \cdot 4H_2O$ crystals modeled by microscopic spin Hamiltonian approach. *J. Magn. Magn. Mater.* **2016**, *401*, 1068–1077, doi:10.1016/j.jmmm.2015.11.007.

16. Brisebois, P.P.; Izquierdo, R.; Siaj, M. Room-Temperature Reduction of Graphene Oxide in Water by Metal Chloride Hydrates: A Cleaner Approach for the Preparation of Graphene@Metal Hybrids. *Nanomaterials* **2020**, *10*, 1255, doi:10.3390/nano10071255.

17. Khandanlou, R.; Ahmad, M.; Shameli, K.; Kalantari, K. Synthesis and Characterization of Rice Straw/Fe_3O_4 Nanocomposites by a Quick Precipitation Method. *Molecules* **2013**, *18*, 6597–6607, doi:10.3390/molecules18066597.

18. Huang, X.; An, D.; Song, J.; Gao, W.; Shen, Y. Persulfate/electrochemical/$FeCl_2$ system for the degradation of phenol adsorbed on granular activated carbon and adsorbent regeneration. *J. Clean. Prod.* **2017**, *165*, 637–644, doi:10.1016/j.jclepro.2017.07.171.

19. Kakar, S.; Batra, D.; Singh, R. Preparation and evaluation of magnetic microspheres of mesalamine (5-aminosalicylic acid) for colon drug delivery. *J. Acute Dis.* **2013**, *2*, 226–231, doi:10.1016/S2221-6189(13)60132-8.

20. Shaghaghi, B.; Khoee, S.; Bonakdar, S. Preparation of multifunctional Janus nanoparticles on the basis of SPIONs as targeted drug delivery system. *Int. J. Pharm.* **2019**, *559*, 1–12, doi:10.1016/j.ijpharm.2019.01.020.

21. Ahmad, T.; Ahmad, K.; Alam, M. Characterization of Water Treatment Plant's Sludge and its Safe Disposal Options. *Procedia Environ. Sci.* **2016**, *35*, 950–955, doi:10.1016/j.proenv.2016.07.088.

22. Kang, S.; Sun, Y.; Deng, S.; Li, S.; Su, Y.; Guo, W.; Li, J. Extraction of Huadian oil shale in subcritical $FeCl_2$ solution. *Fuel Process. Technol.* **2021**, *211*, 106571, doi:10.1016/j.fuproc.2020.106571.

23. Tang, B.; Su, W.; Wang, J.; Fu, F.; Yu, G.; Zhang, J. Minimizing the creation of spent pickling liquors in a pickling process with high-concentration hydrochloric acid solutions: Mechanism and evaluation method. *J. Environ. Manage.* **2012**, *98*, 147–154, doi:10.1016/j.jenvman.2011.12.027.

24. No Title Available online: CONDORCHEM ENVITECH, S. L. (2017). Life Dime HCl & Zn Recovery.

25. Roisnel, T.; Rodriguez-Carvajal, J. WinPLOTR, a graphic tool for powder diffraction.

26. Verbist, J.J.; Hamilton, W.C.; Koetzle, T.F.; Lehmann, M.S. Neutron Diffraction Study of Iron(II) Chloride Tetrahydrate, FeCl2· 4H2O. *J. Chem. Phys.* **1972**, *56*, 3257–3264, doi:10.1063/1.1677688.

27. Guchhait, S.K.; Sammi, H.; Yadav, K.K.; Rana, S.; Jha, M. New hydrometallurgical approach to obtain uniform antiferromagnetic ferrous chloride cubes from waste tin cans. *J. Mater. Sci. Mater. Electron.* **2021**, *32*, 2965–2972, doi:10.1007/s10854-020-05048-1.

28. Cariati, F.; Masserano, F.; Martini, M.; Spinolo, G. Raman studies of $NiX_2 \cdot 6H_2O$ and $FeCl_2 \cdot 4H_2O$. *J. Raman Spectrosc.* **1989**, *20*, 773–777, doi:10.1002/jrs.1250201204.

29. Caswell, N.; Solin, S.A. Vibrational excitations of pure $FeCl_3$ and graphite intercalated with ferric chloride. *Solid*

State Commun. **1978**, *27*, 961–967, doi:10.1016/0038-1098(78)91015-3.

30. de Faria, D.L.A.; Venâncio Silva, S.; de Oliveira, M.T. Raman microspectroscopy of some iron oxides and oxyhydroxides. *J. Raman Spectrosc.* **1997**, *28*, 873–878, doi:https://doi.org/10.1002/(SICI)1097-4555(199711)28:11<873::AID-JRS177>3.0.CO;2-B.

31. Nieuwoudt, M.K.; Comins, J.D.; Cukrowski, I. The growth of the passive film on iron in 0.05 M NaOH studied in situ by Raman micro-spectroscopy and electrochemical polarisation. Part I: Near-resonance enhancement of the Raman spectra of iron oxide and oxyhydroxide compounds. *J. Raman Spectrosc.* **2011**, *42*, 1335–1339, doi:10.1002/jrs.2837.

32. Criado, M.; Martínez-Ramirez, S.; Bastidas, J.M. A Raman spectroscopy study of steel corrosion products in activated fly ash mortar containing chlorides. *Constr. Build. Mater.* **2015**, *96*, 383–390, doi:10.1016/j.conbuildmat.2015.08.034.

33. Gilberg, M.R.; Seeley, N.J. The identity of compounds containing chloride ions in marine iron corrosion products: a critical review. *Stud. Conserv.* **1981**, *26*, 50–56, doi:10.1179/sic.1981.26.2.50.

34. Neff, D.; Bellot-Gurlet, L.; Dillmann, P. Deterioration of iron archaeological artefacts: micro-Raman investigation on Cl-containing corrosion products. **2007**, doi:10.1002/jrs.1659.

35. Bull, J.N.; Maclagan, R.G.A.R.; Fitchett, C.M.; Tennant, W.C. A new isomorph of ferrous chloride tetrahydrate: A 57Fe Mössbauer and X-ray crystallography study. *J. Phys. Chem. Solids* **2010**, *71*, 1746–1753, doi:10.1016/j.jpcs.2010.09.009.

36. Murad, E. Magnetic properties of microcrystalline iron (III) oxides and related materials as reflected in their Mössbauer spectra. *Phys. Chem. Miner.* **1996**, *23*, 248–262, doi:10.1007/bf00207766.